Boundary-Layer Profile Measurements in a Combustion Driven MHD Generator

John W. Daily,* C.H. Kruger,† S.A. Selft, ‡ and R.H. Eustis†
Stanford University, Stanford, Calif.

The velocity, temperature, and electron number density profiles were measured in the electrode wall boundary layer of a combustion driven MHD generator. Both subsonic and supersonic conditions were run. The experimental results are compared with predictions of a two-dimensional turbulent boundary-layer computation. For the subsonic condition, high levels of freestream turbulence were measured, about 10-12%. The measured velocity profile was fatter than that predicted, although the temperature and electron number density profiles were in agreement. This difference is tentatively ascribed to the high freestream turbulence levels. There was no measurable MHD effect for the subsonic case. For the supersonic condition, the measured velocity, temperature, and electron number density profiles fell under the predicted profiles. The discrepancy may be due to three-dimensional recirculation effects. There was a small amount of MHD interaction, the degree of which was in agreement with predictions. Electron number density nonequilibrium was not identified, but the degree of nonequilibrium predicted was small. Under the appropriate supersonic conditions, primarily at freestream temperatures below 2400K, ionization nonequilibrium is predicted to occur.

Nomenclature

A^+, A_0^+ = Van Driest constants
A_e, A_i = electron and ion number fluxes
$A_{k\ell}$ = Einstein A coefficient
$\boldsymbol{B}, B_z$ = magnetic field vector and z component
B_ν = Planck function
$\bar{C}_e, C_e'$ = average and fluctuating parts of electron concentration
C_p = mixture specific heat
D = Van Driest damping function
D_a = ambipolar diffusion coefficient
Dir = constant in pressure gradient equation
e = electron charge
$\boldsymbol{E}$ = electric field vector
g_i^+, g_k = potassium ion and excited atom quantum degeneracies
h = Planck's constant
h, h_s = static enthalpy of mixture and component
$\bar{H}, H'$ = average and fluctuating parts of total enthalpy
I_ν = radiation intensity
J = electric current density
J_s = mass flux of species s
k = Boltzmann constant
K = mixing length constant
K_s = species mass fraction
ℓ_m, ℓ_D = momentum and heat and mass transfer mixing lengths
Le_s = species Lewis number
L_{op} = optical path length
m_e = electron mass
N_e = electron number density
N_k = excited potassium level number density
p = static pressure
P^+, P_E^+ = Van Driest constants

$$P^+ = \frac{\mu}{\rho^{1/3}\tau_w^{2/2}}\left(\frac{dp}{dx} - J_y B_z\right)$$

Pr, Pr_t = normal and turbulent Prandtl numbers
q_y = y component of energy flux
T = static temperature
T_L = lamp temperature
T_R = reversal temperature
$\bar{u}, u'$ = average and fluctuating x velocity component
$\bar{v}, v'$ = average and fluctuating y velocity component
$\bar{w}, w'$ = average and fluctuating z velocity component
x, y, z = spatial coordinates (Fig. 1)
y^+ = $y(\rho\tau_w/\mu)^{1/2}$
α = thermal diffusivity $\lambda/\rho C_p$
δ_{99} = 99% momentum boundary-layer thickness
δ_{sw} = sidewall boundary-layer thickness
$\epsilon_m, \epsilon_H, \epsilon_e, \epsilon_D$ = eddy diffusivities
ϵ_λ = ionization energy for level k
λ = thermal conductivity
μ = dynamic viscosity
μ_{eff} = effective viscosity
μ_e, μ_i = electron and ion mobility
ν = frequency
ρ = mass density
τ = optical depth
τ_{yx} = shear stress

I. Introduction

THREE of the most important losses in MHD generators are boundary-layer phenomena: friction, heat transfer, and boundary-layer voltage drop. The boundary layers on the channel walls are turbulent and, in the transonic and supersonic case, strongly influenced by compressibility effects. Variable transport properties are important, and body forces and Joulean heating can alter the growth of the boundary layer. High levels of freestream turbulence, driven by the combustion process, may have a direct effect on turbulent momentum transport and friction losses. For supersonic MHD channels, the high velocity coupled with turbulence gives rise to finite chemical reaction rate effects. As a result, the energetics of the boundary layer are modified, affecting

Received Oct. 31, 1975; revision received March 24, 1976. The work reported in this paper was supported by the AeroPropulsion Laboratory, Wright-Patterson Air Force Base, under Contract No. AFAPL F-33615-72-C-1088, by the National Science Foundation, Grant NSF AER-72-03487 and by the Energy Research and Development Agency, Contract DI-14-32-0001-1739. The authors acknowledge with gratitude the assistance of J.K. Koester, F. Levy, and F. Reigel in conducting the experimental work.

Index category: Plasma Dynamics and MHD.

*Presently: Assistant Professor of Mechanical Engineering, University of California, Berkeley, Calif. Member AIAA.

†Professor of Mechanical Engineering. Member AIAA.

‡Professor of Mechanical Engineering.

wall heat transfer rates. In addition, the finite electron-ion recombination rate may become important in the supersonic boundary layer. Electron number density, and thus electrical conductivity, may be substantially different than that predicted by equilibrium considerations. (Chemical nonequilibrium is discussed in Ref. 1.)

Because of the nature of these processes, it is especially difficult to infer knowledge about them from the gross behavior of the generator. The information of most value to an understanding of the basic physics are the profiles of the dependent variables. In this study velocity, temperature, and electron number density are considered. (This is not true in the case of chemical nonequilibrium, which has little effect on temperature profiles but may change the heat transfer rate by a factor of two.[1])

Numerous workers have studied MHD flows theoretically, although only a few have studied combustion gas or combustion gas-like flows. Teno, Lui, and Brogan[2] studied aerodynamic effects of boundary layers in MHD generators using integral techniques. They showed that electrode wall boundary-layer separation is important in determining supersonic channel performance.

Cott[3] considered the insulator walls of a potassium-seeded nitrogen MHD accelerator. Although the flow was laminar, significant ionizational nonequilibrium was predicted near the walls. This may have been due to the very large velocities considered ($u = 3000$-5500 m/sec.). He considered a collisionless sheath and solved the boundary-layer equations using the method of Patankar and Spalding.[4] High and Felderman[5] extended the work of Cott[3] to turbulent flow. They showed that, although electron energy nonequilibrium may not be significant, ionizational nonequilibrium is important for the conditions considered.

Argyropoulos et al.[6] studied electron energy nonequilibrium in combustion-driven MHD generators. They concluded that at large current densities and at current concentrations electron energy nonequilbirum is important only very near the electrodes. Daily, Raeder, and Zankl[1] studied chemical nonequilibrium effects in a combustion-driven MHD generator. Comparison of limit calculations with heat transfer data indicate that supersonic flows can be frozen energetically.

There have been numerous cases of profile measurements in both laminar and turbulent, low-temperature, boundary-layer flows, but there have been few such measurements in hot MHD flows. An early reported work is that of Brederlow, Lengyel, and Zinko,[7] who measured velocity and temperature profiles in the y-z plane of a potassium-seeded argon plasma generator. They used a pitot probe to measure velocity and a thermocouple probe coupled with line-reversal measurements to measure temperature. They used the results to study the effect of boundary layers on open-circuit voltage. Several other workers have made both probe and spectroscopic measurements in noble gas flows,[8-10] but only Olin[11] has made such measurements in a fully developed combustion flow. He measured velocity profiles in an insulated channel using a water-cooled pitot probe. By turning on a magnetic field he could study turbulence suppression due to MHD body forces.

Although there has been work done in the area of high-temperature combustion gas boundary layers, there is little such work which is directly applicable to the present study. Also, there is no reported work in which velocity, temperature, or electron number density profiles were measured in the developing flow, combustion driven MHD power generator.

The paper is organized as follows: Sec. II provides a description of the theoretical model; Sec. III describes the experimental facility and methods used in measuring velocity, temperature, and efectron number density profiles; Sec. IV discusses the results of the experiments; and Sec. V states the conclusions reached by the study.

II. Theory

A. Assumptions

The flow modeled is the growth of an internal turbulent boundary layer in the x-y symmetry plane of the confined MHD duct (Fig. 1). Although the flow in an MHD duct is inherently three-dimensional, the flow in the plane considered is approximately two-dimensional. Three-dimensional effects appear in two ways: first, the mass flux will change as the flow expands or contracts in the channel; second, turbulent recirculation may occur. For the plane in question, this would involve a transport of low-momentum fluid into the plane near the wall and high-momentum fluid out of the plane in the freestream. This effect is neglected in the theoretical study, but experimental results indicate it may be important in a real flow. Variable mass flux is accounted for through the continuity equation. Pressure gradients in the y direction are not important in these studies. Variable thermodynamic and transport properties are included in the model. Turbulence suppression, which may be important at higher values of magnetic field, may be ignored in the present study.

The continuity, momentum, total enthalpy, and electron-ion continuity equations are solved. The electron temperature is assumed equal to the gas temperature. Due to the difficulty of complete treatment chemical nonequilibrium is considered only in the limits of frozen and equilibrium flow. Calculations[1] indicate that nonequilibrium may be important in determining heat transfer rates; however, the effect on the temperature profile itself is minimal. The basic equations are derived using the traditional Reynolds decomposition and taking the mean of the resulting expressions.

B. Constitutive Relations

The constitutive relations for the molecular transport of momentum, mass and species are taken from Hirschfelder, Curtiss, and Bird.[12] (Ch. VII). Reduced to boundary-layer form, they become:

momentum: $$\tau_{yx} = \mu \frac{\partial \bar{u}}{\partial y} \tag{1}$$

energy: $$q_y = -\frac{\lambda}{C_p}\left\{\frac{\partial h}{\partial y} + \sum_s (Le_s - 1) h_s \frac{\partial K_s}{\partial y}\right\} \tag{2}$$

where Le_s = species Lewis number is taken as unity in this study.

Species:

$$J_s = -\mu_s\left\{\pm \rho_s E_y - \frac{\partial}{\partial y}\left(\frac{\rho_s k T}{e}\right)\right\} \tag{3}$$

where + is for electrons.

C. Turbulence Closure

The turbulence mixing terms are modeled using the eddy viscosity and mixing length concepts coupled with empirical correlations developed by Kays.[13] Also, because the experimental results indicate a high level of freestream turbulence for the subsonic conditions, corrections for such effects suggested by the work of McDonald[14] are included.

The turbulence fluxes are assumed to be of the form

$$-\overline{\rho u' v'} = \bar{\rho}\epsilon_m (\partial \bar{u}/\partial y) \quad \text{(Momentum)} \tag{4}$$

$$-\overline{\rho H' v'} = \bar{\rho}\epsilon_H (\partial \bar{H}/\partial y) \quad \text{(Energy)} \tag{5}$$

$$-\overline{\rho C_e' v'} = \bar{\rho}\epsilon_e (\partial \bar{C}_e/\partial y \quad \text{(Electrons)} \tag{6}$$

The eddy viscosities are assumed to be of the form

$$\epsilon_m = \ell_m^2 \frac{\partial \bar{u}}{\partial y} \tag{7}$$

for momentum, and

$$\epsilon_H = \epsilon_e = \ell_D^2 \frac{\partial \bar{u}}{\partial y} \equiv \epsilon_D \tag{8}$$

for diffusion of heat and mass, where ℓ_m and ℓ_D are the mixing lengths for turbulent momentum and heat and mass transport, respectively, and the turbulent Lewis number (ϵ_e/ϵ_H) is assumed to be unity.

The functional form of the mixing length is shown in Fig. 2. In the laminar sublayer, ℓ is small. In the middle, highly turbulent region, ℓ grows linearly out to the wake region, where it remains at a constant value. The value at which the momentum mixing length stops growing is dependent on the amount of freestream turbulence. Kays[13] shows that 0.085 δ_{99} is a reasonable value for low freestream turbulence levels. For high levels of freestream turbulence, δ_{99} or a channel dimension must be the limiting value of ℓ_m[14]. Figure 3 compares velocity profiles calculated using different cutoff y/δ values for ℓ_m, and, as can be seen, the effect is significant. McDonald[14] suggests that unlike momentum, heat and mass transport are little affected by freestream turbulence. Thus, a slower cutoff may be necessary for the heat and mass transport mixing lengths. In the present study, cutoff values were used which seemed best to fit the data.

The momentum mixing length is described in the inner region by the relation $\ell_m = KyD$, where K is a constant (0.41 in this study) and D is the Van Driest damping function, $D = 1 - e^{(-y^+/A^+)}$. A^+ may be throught of as the nondimensional laminar sublayer thickness and as such will be found to be affected by pressure gradients. In this analysis, A^+ is calculated following Kays[3]

$$A^+ = \frac{A_0^+}{30.2\,P_E^+ + 1} \tag{9}$$

where A_0^+ is the zero-pressure gradient A^+ (24.0 here) and P_E^+ is an effective pressure gradient parameter. P_E^+ is the solution of the ordinary differential damping equation

$$\frac{dP_E^+}{dx} = -\frac{P_w(\tau_w/\rho_w)^{1/2}}{4000\,\mu_w \mathrm{Dir}}(P_E^+ - P^+) \tag{10}$$

where Dir = 0.1 for $P^+ > P_E^+$ and 1.0 for $P^+ \le P_E^+$.

For smooth wall boundary layers and low freestream turbulence, the two mixing lengths can be related through a turbulent Prandtl number

$$Pr_t = \epsilon_m/\epsilon_D = (\ell_m/\ell_D)^2 \tag{11}$$

Kays[13] has found the turbulent Prandtl number to vary as

$$Pr_t = 1.43 - 0.17(y^+)^{1/4}, \quad Pr \le 0.85 \tag{12}$$

otherwise $Pr_t = 0.85$. When freestream turbulence is present, the momentum mixing length which would occur without freestream turbulence is used to calculate ℓ_D.

D. Governing Equations

Incorporating the previous, the governing equations become

Continuity:

$$\frac{\partial \overline{\rho u}}{\partial x} + \frac{\partial \overline{\rho v}}{\partial y} + \frac{\partial \overline{\rho w}}{\partial z} = 0 \tag{13}$$

Momentum:

$$\overline{\rho u}\frac{\partial \bar{u}}{\partial x} + \overline{\rho v}\frac{\partial \bar{u}}{\partial y} = \frac{\partial}{\partial y}\left((\mu + \bar{\rho}\epsilon_m)\frac{\partial \bar{u}}{\partial y}\right) - \frac{\partial \bar{p}}{\partial x} + (J \times B)_x \tag{14}$$

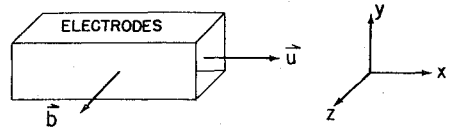

Fig. 1 MHD coordinate system.

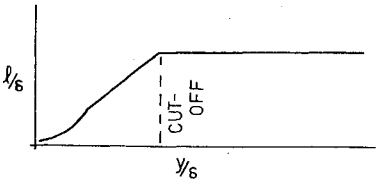

Fig. 2 Mixing length.

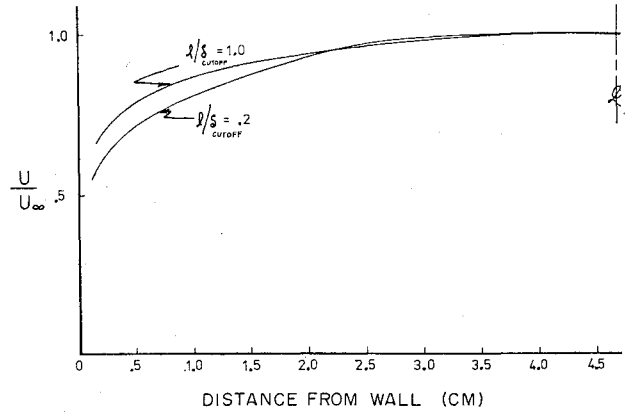

Fig. 3 Effect of mixing length cutoff on velocity profile.

Energy:

$$\overline{\rho u}\frac{\partial \bar{H}}{\partial x} + \overline{\rho v}\frac{\partial \bar{H}}{\partial y} = \frac{\partial}{\partial y}\left(\frac{\mu}{Pr}\left(1 + \frac{\epsilon_D}{\alpha}\right)\frac{\partial \bar{H}}{\partial y}\right) + \frac{1}{2}\frac{\partial}{\partial y}\left(\mu\left(1 - \frac{1}{Pr}\right)\frac{\partial \bar{u}^2}{\partial y}\right) + J \cdot E \tag{15}$$

Electron-Ion Continuity:

$$\overline{\rho u}\frac{\partial \overline{C_e}}{\partial x} + \overline{\rho v}\frac{\partial \overline{C_e}}{\partial y} = \frac{\partial}{\partial y}\left(\bar{\rho}(D_a + \epsilon_D)\frac{\partial \overline{C_e}}{\partial y}\right) + R_e \tag{16}$$

where the electron and ion continuity equations have been combined to eliminate the electric field and D_a is the ambiopolar diffusion coefficient. These equations, plus an equation of state and the appropriate initial and boundary conditions, provide a complete description of the problem as considered.

The equation of state relation $h = h(p,T)$ and the transport properties are calculated following Pepper.[15] The equation of state relations are calculated in the equilibrium case using a conventional equilibrium calculation. For the case of chemically frozen boundary layers, it is assumed that the equilibrium relations hold in the freestream. Across the boundary layer, however, C_p is fixed at its freestream value and the relation $dh = C_p dT$ used to evaluate the temperature.

E. Initial Conditions

For the purpose of starting the calculations, the freestream velocity and temperature are assumed given at some position downstream of the throat (see Fig. 4), usually at the first static pressure tap in the actual channel. A simple three-layer model similar to that of Martinelli[16] is used for the initial velocity profile, and the total enthalpy and electron number density profiles are assumed to be similar to that of velocity.

The information available to determine the freestream conditions at the first static pressure tap are the local static pressure, the mass flow rate, the chemical composition and total pressure in the plenum chamber upstream of the nozzle, and the total pressure at the downstream end of the channel, which is measured by a pitot probe.

The initial freestream conditions may be calculated by assuming that an isentropic expansion takes place between the plenum total pressure and the static pressure at the start of the channel, using the calculated adiabatic flame temperature (corrected for heat transfer) as the total temperature. Differences between these ideal initial conditions and the initial conditions based on the channel pressure, mass flux, and probe stagnation pressure are an indication of apparent nozzle and combustion efficiencies.

F. Boundary Conditions

The boundary conditions for the momentum and energy equations are respectively

$$U(x,0)=0, \qquad \frac{\partial u}{\partial y}(x,y_{\ell})=0$$

$$T(x,0)=T_w, \qquad \frac{\partial H}{\partial y}(x,y_{\ell})=0$$

Electron-Ion Continuity Boundary Conditions

The electron-ion continuity equation is valid in the bulk of the plasma but fails very close to wall because it does not treat either the Knudsen layer or the sheath region. However, it does describe the ionization nonequilibrium region, to which charged particles can diffuse at a rate faster than they can recombine.

In the absence of a detailed analysis of the near electrode region, an approximate method[8,17] is used to derive a boundary condition based on the following assumptions: a) all charged particles that impinge on the electrode are absorbed, and there is no emission of charged particles; b) the sheath is thinner than the Knudsen layer, and thus is collisionless; c) the electrode potential is less than plasma potential at the edge of the Knudsen layer.

Subject to the previous assumptions the boundary condition is valid for the anodes at current densities up to about 1 A/cm^2. Only the anode is treated in the present work. The boundary condition is obtained by matching the ion and electron fluxes on either side of the Knudsen layer. This yeilds[8,17]:

$$-\frac{\partial}{\partial y}\left(\frac{N_e kT}{e}\right)=\frac{1}{2}\left\{\frac{N_e\overline{C_i}}{2\mu_i}-\frac{J_w/e}{\mu_e}\right\} \tag{17}$$

where μ_e and μ_i are the electron and ion mobilities, J_w is the current density at the wall, e the charge on an electron, and $\overline{C_i}$ the ion thermal velocity at the wall.

The assumption of a collisionless sheath is not exactly correct in combustion plasmas. However, the collisionless assumption yields a very simple form, whereas the correct boundary condition would require separate numerical solution of simultaneous differential equations. Furthermore, numerical studies indicate that the calculated electron number density profiles are very insensitive to the exact form of the boundary condition at distances greater than 1-3% of the boundary-layer thickness. This is due to the low wall temperatures of the present study; any low value of N_e at the wall will result in a reasonable solution. The collisionless sheath model is not satisfactory for calculation of voltage drop.

G. Electron-Ion Continuity Source Term

The source term $\dot{R}_e$ used in the electron-ion continuity equation is that of Curry,[18] uncorrected for turbulence effects. Curry's model is based on collisional theory and has been corrected for combustion gases. As discussed in Ref. 19, the proper recombination rate to use in analyzing turbulent flows is the time-average value. Since we do not have any way to calculate the true time-average rate, we instead evaluate Curry's[18] results using the average values of electron number density and temperature. The expression used is

$$\alpha=2.519\times 10^{-33}N_e(m^{-3})\,e^{-2.98\times 10^{-3}T(\mathrm{K})} \quad (M^3/\mathrm{sec}) \tag{18}$$

and the source term for the electron ion continuity equation becomes

$$\dot{R}_e=m_e\dot{N}_e=m_e\alpha(N_e^{*2}-N_e^2) \tag{19}$$

where the star indicates that the equilibrium value of N_e is to be used.

H. Numerical Method

The problem as formulated requires solution of three simultaneous, parabolic, partial differential equations with associated initial and boundary conditions. The solution procedure, somewhat similar to that of Patankar and Spalding,[4] consists of transforming the coordinate system, approximating the resulting equations with linearized finite difference equations, and solving the resulting linear system numerically. The details are discussed fully in Ref. 19.

III. Experimental Apparatus and Methods

A. Experimental Apparatus

The boundary-layer experiments were made in the Stanford M-8 MHD facility, designed specifically for boundary-layer studies. A schematic of the system is shown in Fig. 5 with the principal dimensions.

Fuel, oxidizer, and nitrogen diluent are mixed and burned in a swirl-stabilized combustor. The combustion gases then pass into a large plenum chamber, where combustion is completed and nonuniformities allowed to decay. From the plenum the gases pass through a nozzle into a 0.6-m-long run-in section and a 0.7-m MHD section. The channel is water-cooled stainless steel lined with MgO ceramic. There are 22 electrode pairs connected in the segmentated Faraday mode. The flat electrodes, 2.25 cm long in the flow direction with a pitch of 3 cm, extend completely across the channel. The electrode material is also stainless steel.

The run-in section, added to enhance boundary-layer growth, is designed for a constant Mach number of about 1.7, but may also operate at subsonic velocities. The MHD section is designed to operate at approximately constant pressure under conditions of maximum interaction. Boundary-layer measurements are made 1.2 m from the nozzle under electrode #20. The boundary layers are about 2-cm thick at this location.

B. Experimental Measurements

The gas temperature and electron number density were both measured spectroscopically.

Gas Temperature

The gas temperature was measured using the sodium D-line wing-reversal method, which has been well-documented by Brederlow et al.[20] This method consisted of illuminating the plasma with a light source of known intensity. The radiative transfer equation may then be written

$$I_\nu(L)=I_{\nu_{\mathrm{PLASMA}}}+e^{-\tau}B_\nu(T_L) \tag{20}$$

where $I_{\nu_{\mathrm{PLASMA}}}$ is the intensity of radiation from the plasma alone, $B_\nu(T_L)$ is the Plank function, and T_L is an equivalent black body temperature for the light source. The reversal temperature is defined as $T_R=T_L$ when:

$$I_{\nu_{\mathrm{PLASMA}}}=(1-e^{-\tau})B_\nu(T_g) \tag{21}$$

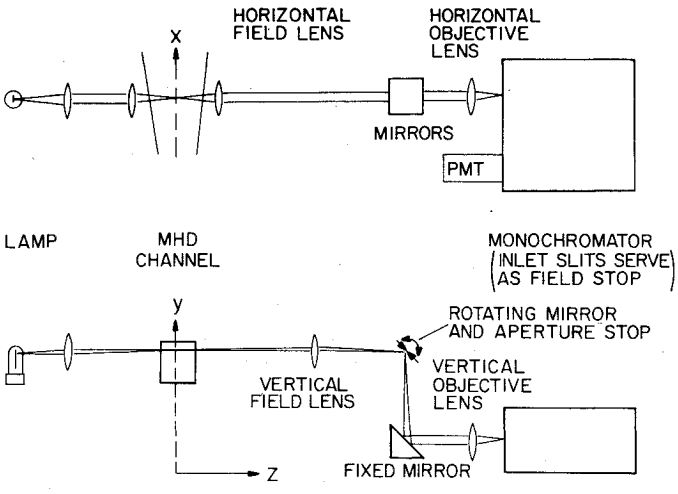

Fig. 4 M-8 MHD facility.

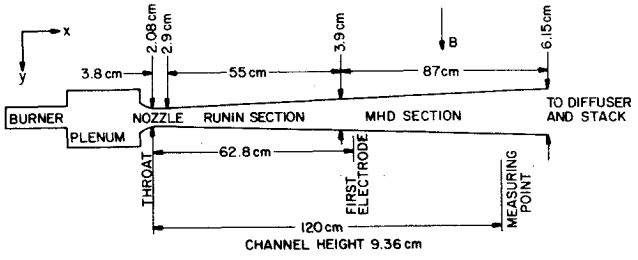

Fig. 5 Optical scanning system.

Therefore $T_R \equiv T_g$. In the case of a nonuniform plasma with cold sidewall boundary layers, however, the reversal temperature may be significantly reduced below the centerline gas temperature. A correction for this effect was obtained from a numerical solution of the equation of radiative transfer using the calculated sidewall temperature distribution along the line of sight (see Ref. 21).

Electron Number Density

Electron density was measured using the higher-lying energy states of the potassium atom, as discussed by McGregor.[22] For sufficiently high levels, processes which either ionize the atom or cause transition to a nearly level become much more important than either radiative processes or processes which result in transitions to lower-lying levels. As a result, the higher levels are in Boltzmann equilibrium with each other and in Saha equilibrium with the free electrons.

The higher energy levels undergo radiative transitions to lower levels, and their number density can be related to the radiation field through the radiative transfer equation:

$$\hat{I}(L) = \int_0^L h\nu \frac{A_{k\ell}}{4\pi} N_k(s)\, ds = h\nu \frac{A_{k\ell}}{4\pi} \hat{N}_k \qquad (22)$$

where $A_{k\ell}$ is the Einstein coefficient for spontaneous emission and N_k is $N_k(s)$ averaged over the optical path. Again the effect of cold sidewall boundary layers is to reduce the average value of N_k below the centerline level.

The centerline number density can be calculated if a number density distribution is assumed. Calculations with the boundary-layer computer program led to the conclusion that under most conditions the variation of N_k with s was nearly linear. This leads to a correction of the form

$$N_{k\infty}/\hat{N}_k = 1/(1-\delta_{sw}/L_{op}) \qquad (23)$$

This value of N_k was used with the excited-level Saha equation

$$N_e^2 = N_k \frac{g_i^+}{g_k} \left(\frac{2\pi m_e kT}{h^2}\right)^{3/2} \exp(-\epsilon_{k\lambda}/kT) \qquad (24)$$

to obtain the experimental value of N_e as a function of distance above the electrode. The potassium 6D (5360 Å) and 7D (5112 Å) lines were used in the present study.

The spectroscopic boundary-layer measurements are made using the optical scanning system shown in Fig. 5. A tungsten lamp is imaged into the plasma for use with the line reversal procedure. Light emitted from the plasma is collimated and sent to a pivot-mounted mirror that also serves as the aperture stop. From the mirror the light is then passed through a second lens and imaged on the entrance slit of the monochromator. Because the mirror is at the focal point of the field lens, only that light which is parallel to the lens axis and whose solid angle and image size are defined by the mirror stop and entrance slit, respectively, will be admitted. Scanning is accomplished by rotating the mirror. Resolution in the y-direction is about 0.3 mm. One unusual aspect of the system is that two-dimensional, cylindrical lenses are used, allowing a large aperture in the x-z plane. Thus, for a given resolution in the y direction, the total solid angle can be maximized. Details of the measurements are discussed in Ref. 19.

Velocity

The velocity profiles are measured using a laser Doppler velocimeter developed at Stanford for combustion MHD flows. The LDV system has been described elsewhere.[23] For the measurement, micron-size, stabilized zirconia particles are injected into the plenum, where they are mixed with the hot gases and carried into the channel. The LDV then measures a time-averaged velocity probability function for the particles which pass the measurement point. This probability distribution function is not necessarily that of the gas. However, calculations indicate that 1-μ zirconia particles should follow the mean flow for both the subsonic and supersonic conditions considered. Thus, to within some uncertainty, the mean velocities and turbulence intensities obtained from the measurements are the same as for the gas. See Ref. 19. The spacial resolution is better than 0.1 mm in the y direction.

Optical access to the MHD channel was provided via windows. The gas temperature and electron number density windows consisted of two slots on opposite sides of the channel and normal to the gas flow. The slots were 0.5-cm wide, 4.0-cm in height, and 5.0 cm deep. The LDV window consisted of a port, 2.5 × 2.5 cm and 10 cm deep, mounted at an angle of 20° to the channel centerline. All windows were capped with quartz flats which were film-cooled with nitrogen purge gas. In addition, pneumatically operated shutters were provided which protected the flats when measurements were not being made.

The uncertainty relations used to calculate the error bars shown on the data reported in the next section are given in Ref. 19.

IV. Stanford M-8 Results and Discussion

A series of experiments were run in the Stanford M-8 MHD channel using stainless steel electrodes. The several tests included a subsonic condition and a supersonic condition, both with and without magnetic field and current. With the cold electrodes it was not possible to achieve high levels of MHD interaction. For the subsonic cases reported there was no measured or calculated effect on the velocity, temperature, and electron density profiles when the magnetic field was applied. The current density was about 0.005 A/cm^2. In the supersonic runs the current density was about 0.5 A/cm^2 and there was a small effect on the profiles, including an increase

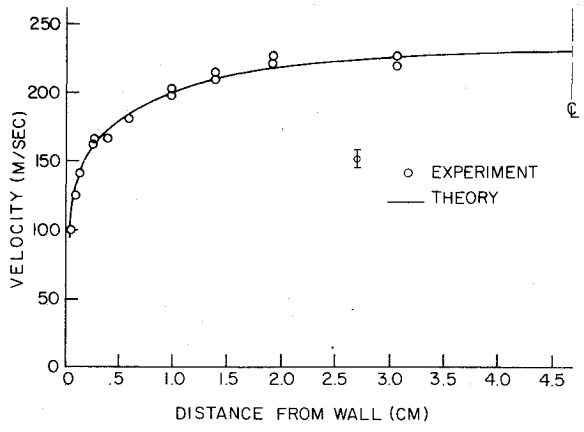

Fig. 6 Gas velocity-subsonic flow.

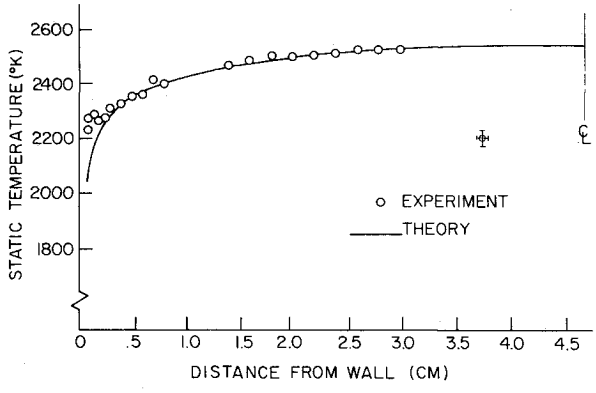

Fig. 7 Static temperature-subsonic flow.

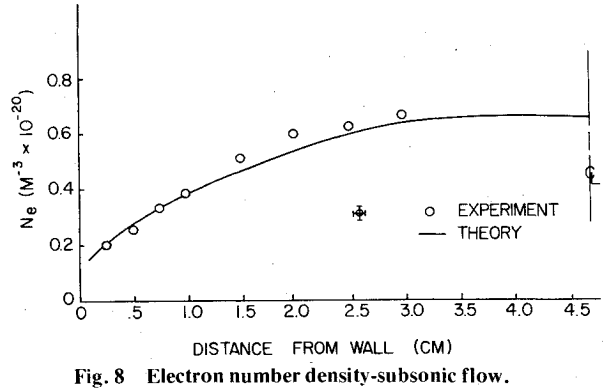

Fig. 8 Electron number density-subsonic flow.

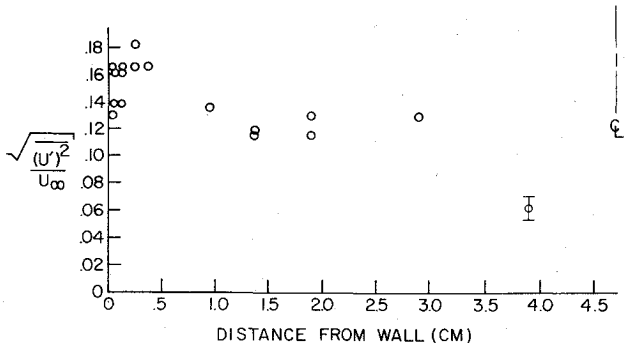

Fig. 9 Turbulent intensity-subsonic flow.

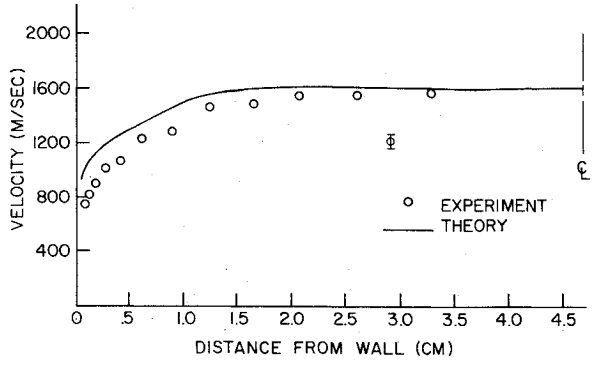

Fig. 10 Gas velocity-supersonic flow, $B=0$.

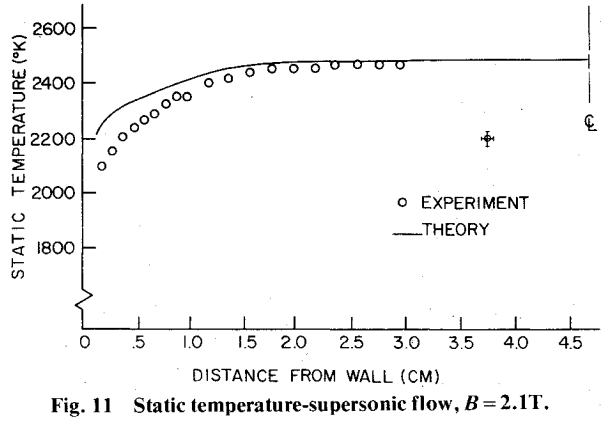

Fig. 11 Static temperature-supersonic flow, $B=2.1$T.

in temperature, the magnitude of which was in agreement with theory.

A. Subsonic Results and Discussion

The subsonic condition obtained was at a freestream Mach number of about 0.225 and diameter and length Reynolds numbers of 2500 and 4.8×10^5, respectively. The measured freestream velocity was 225 m/sec ± 10 m/sec, and the measured freestream static temperature was 2530K ± 30-40K. The wall temperatures were about 1750K for the ceramic linear and 500K for the electrodes. Figures 6-9 show the measured and calculated velocity, temperature, and electron number density profiles and the measured turbulence intensity profile for the subsonic condition.

The initial conditions used were obtained by fixing the upstream static pressure and mass flow rate, both of which were measured, and then setting the initial freestream velocity and temperature (only one of which is then independent) so as to match the measured freestream velocity and temperature downstream. The difference between the values obtained in this way and those obtained using the method described in Sec. II is an indication of a combustion efficiency of 90% and a total pressure loss of about 5%. A combustion efficiency of 90% is lower than expected. The discrepancy may be due to uncertainty in the plenum-nozzle heat loss measurements.

To obtain an indication of the reliability of the temperature data, the line reversal results were compared with emission results. The corrected line reversal data agree to within the experimental uncertainty with the emission data reduced using the method of Hohnstreiter,[24] and also reduced by solving the equation of radiative transfer as for the line reversal (see Ref. 21.)

The reliability of the electron number density profile is indicated by the excellent agreement between the theoretical and experimental profiles, since the theory is predicting, for these subsonic conditions, an equilibrium profile. The magnitude of freestream turbulence is significant. Figure 9 shows a level of 10-22%. The source of these fluctuations is difficult to ascertain. However, observations made while obtaining the LDV data indicate that the fluctuations occur at a fairly low frequency and thus may be caused by combustion phenomena. The sidewall boundary layers are almost fully developed. However, even in fully developed channel flows the normal level of freestream turbulence is about 4-5%.

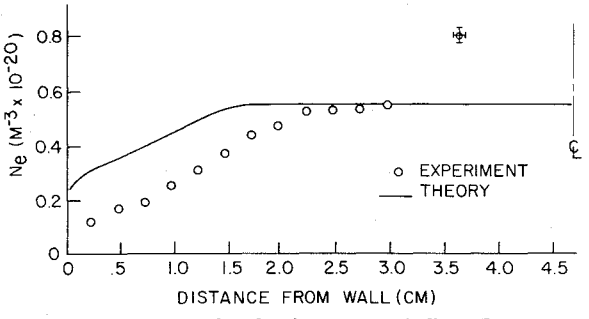

Fig. 12 Electron number density-supersonic flow, $B = 2.1$T.

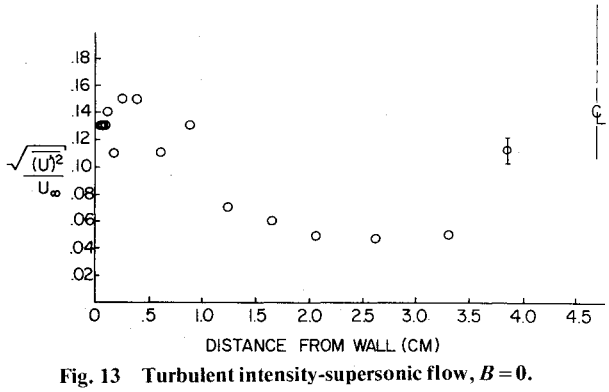

Fig. 13 Turbulent intensity-supersonic flow, $B = 0$.

The apparent agreement between the calculated and measured profiles is due to an adjustment of the momentum mixing length, as discussed in Sec. II. A y/δ cutoff of unity for the momentum mixing length while retaining a y/δ cutoff of 0.085 for the heat and mass mixing length produced the most satisfactory fit to the data. Without this correction, the calculated velocity profile fell well below the measured profile. This effect is consistent with the reported effects of freestream turbulence.[14] That this is most likely so may be seen by considering the fact that of the possible mechanisms which could so substantially influence the velocity profile, all do so in the opposite manner (rough walls, MHD forces, and three-dimensional effects). The calculations indicate that the effect can be responsible for approximately a 25% increase in skin friction coefficient and a 10% increase in Stanton number.

B. Supersonic Results and Discussion

The supersonic condition was run at a freestream Mach number of about 1.6 and a diameter and length Reynolds numbers of 87,500 and 2×10^7, respectively. The measured freestream velocity and static termperature were 1580 m/sec ± 30 m/sec and 2570K ± 30-40K, respectively. The ceramic walls ran at about 2000K and the electrodes at 750K. Figures 10-12 show the measured and calculated velocity, temperature, and electron number density profiles for the supersonic condition. Figure 13 shows the turbulence intensity profile.

The initial conditions used in the calculations were obtained in the same manner as in the subsonic case. The difference between the ideal initial values and those actually used indicates for these conditions a combustion efficiency close to unity and a stagnation pressure loss of about 5%. To obtain an indication of the reliability of the temperature profile, the data were reduced as for the subsonic case. Again, the various methods result in differences less thaan the experimental uncertainty.

For the conditions of the present experiments, the predicted degree of electron nonequilibrium was small. As a result, the difference between the calculated nonequilibrium and equilibrium profiles was smaller than the experimental uncertainty (see Fig. 12). The measured electron density profiles, normalized on the freestream equilibrium N_e, were essentially the same as the equilibrium N_e profiles based on the measured temperatures, to within 5% of the freestream N_e. Thus, to within experimental uncertainty, the measured and calculated profiles are in agreement in indicating a low degree of nonequilibrium for these conditions.

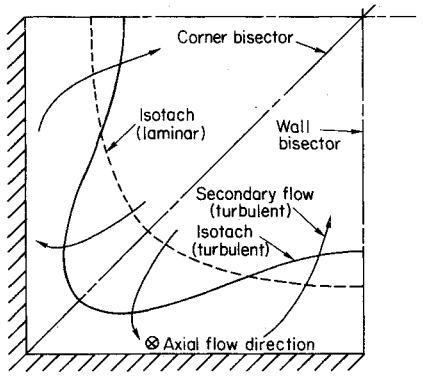

Fig. 14 Typical isotach patterns in a square channel.

To obtain an indication of the reliability of the absolute N_e measurements in both supersonic and subsonic cases, the freestream N_es based on each of two different emission lines and from each of the several experiments were compared with the equilibrium N_es calculated at the measured temperature. The mean of $N_{e_{meas}}/N_e^*(T_{meas})$ is 1.1 with a standard deviation of 0.16. This agreement to within 10% supports normalization of the profiles for comparison of experiment and theory.

The agreement between the experimental and theoretical profiles is not nearly as satisfactory as for the subsonic case. The level of freestream turbulence is much lower than in the subsonic case and was not accounted for in the calculations, but this effect is not sufficient to explain the rapid dropoff with decreasing y of all three measured quantities. One possible explanation of the discrepancy is that at the higher Reynolds numbers of supersonic flow turbulent recirculation becomes important. (In addition, the presence of undetected shocks may have the same effect, although one would normally expect a thickening of the velocity boundary layer as well as a fattening of the temperature profile.) The fact that all three profiles display the same effects tends to support the conclusion that the effect is not caused by experimental error.

As discussed in Sec. II, the flow in the x-y plane along the centerline of the channel is not strictly two-dimensional. In developing turbulent channel flow there exists a transverse mean recirculation flow superimposed on the axial mean flow. This secondary flow has a direct effect on the mean velocity, temperature, and electron number density profiles. Figure 14, taken from Gessener and Jones[25] illustrates this effect. High-momentum fluid is carried down the corner bisectors. The flow turns out along the wall toward the centerline where low-momentum fluid is carried out into the core.

The present experiments were conducted at diameter Reynolds numbers of 2500 and 87,500 for the subsonic and supersonic flows, respectively. Although there is no clear way of determining the exact point where recirculation becomes important, it appears from the literature[25-29] that the effect should not be too large for the low Reynolds number of the subsonic case, but may be very important in the supersonic case.

One mechanism that could depress the velocity profile is surface roughness. However, the work of both Healzer et al.[30] and Pimenta et al.[31] indicates that even in the fully rough case the temperature profile is relatively unaffected, whereas in the present case the measured temperature profiles are substantially below the calculated profiles. Possible sources of error in the velocity profile could be particle slip or

misinterpretation of the particle distribution function. Both effects, however, would appear only to increase the discrepancy between the theory and data.

In summary, it appears reasonable that recirculation effects cannot be ignored for high Reynolds number flows and may be the major factor in explaining the difference between the theoretical and experimental profiles in the supersonic case. It is also possible that dilation due to diverging sidewalls may be important although this effect has not been examined. It also appears that ionizational nonequilibrium is not significant in the present experiment, but calculations indicate that for the supersonic case a significant degree of electron nonequilibrium in the region accessible to measurement would occur for a freestream temperature approximately 100 K below that of the present experiment.

V. Summary and Conclusions

A study of the developing flow in both subsonic and supersonic MHD power generators has been performed. Measurements of electrode wall velocity, temperature, and electron number density profiles have been compared with state-of-the-art, two-dimensional boundary-layer calculations. The study represents the first step in understanding such flows, and several interesting conclusions have been reached which should help direct future work.

For low Reynolds number, subsonic flows in rectangular channels, the flow may be considered quasi-two-dimensional. For high levels of freestream turbulence, there is a strong influence on momentum transfer in the boundary layer which causes steeper velocity profiles and increased calculated skin friction ($\sim 25\%$ in the present case). The agreement between calculated and measured profiles improved once freestream turbulence was corrected for by increasing the momentum mixing length in the outer region of the boundary layer.

The agreement between the calculated and measured profiles in the supersonic case is less satisfactory. The discrepancy is tentatively ascribed to three-dimensional recirculation effects. The integral effect of such recirculation on heat transfer rates, however, is indicated to be small by previous results (Ref. 1), which show only small differences between a round and a square channel.

Electron number density nonequilibrium was not identified, but the degree of nonequilibrium predicted was small. Under the appropriate supersonic conditions, however, ionizational nonequilibrium is expected to occur, particularly since the effect of turbulence would be to reduce the time-averaged recombination rate (see Ref. 19). Our own preliminary rapid-expansion experiments[19] as well as those of Coney,[32] also performed with combustion products, demonstrate the existence of electron nonequilibrium in combustion plasmas.

The difficulties in interpreting the present results illustrate the need for more comprehensive measurements. For example, to examine the 3-D recirculation effect in detail would require measurement of velocity components normal to the walls. The experimental difficulties associated with even the reported measurements, however, cannot be overemphasized.

References

[1]Daily, J.W., Raeder, J., and Zankl, G., "The Effect of Finite Chemical Reaction Rates on Heat Transfer to the Walls of Combustion Driven Supersonic MHD Generator Channels," *AIAA Journal,* Vol. 12, March 1974, pp. 403-404.

[2]Teno, J., Liu, C., and Brogan, T.R., "Boundary Layers in MHD Generators," *Proceedings of the 10th Symposium on Engineering Aspects of MHD,* Cambridge, Mass., 1969, pp. 15-21.

[3]Cott, D.W., "Ionizational and Electron Thermal Nonequilibrium in MHD Boundary Layers," *AIAA Journal,* Vol. 9, Dec. 1971, pp. 2404-2410.

[4]Patankar, S.V. and Spalding, D.B., "A Finite Difference Procedure for solving the Equations of the Two-dimensional Boundary Layer," *International Journal of Heat Mass Transfer,* Vol. 10, Oct. 1967, p. 1389; also Patankar, S.V. and Spalding, D.B., *Heat and Mass Transfer in Boundary Layers,* Interex, London, 1970.

[5]High, M.D., and Felderman, F.J., "Turbulent MHD Boundary Layers with Electron Thermal Nonequilibrium and Finite Rate Ionization," *AIAA Journal,* Vol. 10, Jan. 1972, pp. 98-103.

[6]Argyropoulos, G.S., Demetriades, G.T., Dass, E.D., and Oliver, D.A., "Electron Nonequilibrium in Open-Cycle MHD Generators," *AIAA Journal,* Vol. 12, May 1964, pp. 669-671.

[7]Brederlow, G., Lengyel, L.L, and Zinko, H., "Reduction of the Open-Circuit Voltage by Boundary Layer Leakage Currents in Experimental Faraday Type MHD Generators," 4th International Conference on MHD Electric Power Generation, Warsaw, 1968.

[8]Brown, R.T., "Electron Temperature and Number Density Measurements in a Nonequilibrium Plasma Boundary Layer," Institute for Plasma Research, Stanford Univ., Stanford, Calif., Rept. 350, Jan. 1970.

[9]Tseng, R.C. and Talbot, L., "Flat Plate Boundary Layer Studies in a Partially Ionized Gas," *AIAA Journal,* Vol. 9, July 1971, pp. 1365-1372.

[10]March, W.F.H., "On the Fully Developed Turbulent Compressible Flow in an MHD Generator," Ph.D. Thesis, De Technische Hogeschool, Eindhoven, The Netherlands, 1972.

[11]Olin, J.G., "Turbulence Suppression in Magnetohydrodynamic Flows," Institute for Plasma Research, Stanford University, Stanford, Calif., Rept. 85, July 1966.

[12]Hirschfelder, J.O., Curtiss, C.F., and Bird, R.B., *Molecular Theory of Gases and Liquids,* Wiley, New York, 1954.

[13]Kays, W.M., "Heat Transfer to the Transpired Turbulent Boundary Layer," Dept. of Mechanical Engineering, Stanford Univ. Stanford, Calif., Rept. HMT-14, June 1971.

[14]McDonald, H. and Kreskovsky, J., "Effect of Free Stream Turbulence on the Turbulent Boundary Layers," *International Journal of Heat Mass Transfer,* Vol. 17, July 1974, pp. 705-716; also private communication.

[15]Pepper, J.W., "Effect of Nitric Oxide Control on MHD-Stream Power Plant Economics and Performance," Institute for Plasma Research, Stanford Univ., Stanford, Calif., Rept. 614, Dec. 1974.

[16]Martinelli, R.C., *Transactions of the A.S.M.E.,* Vol. 69, 1947.

[17]Mitchner, M. and Kruger, C.H., *Partially Ionized Gases,* Wiley-Interscience, New York, 1973.

[18]Curry, B.P., "Collisional Radiative Recombination in Hydrogen Plasmas and in Alkali Plasmas," *Phys. Rev. A,* Vol. 1, 1970, pp. 166-176; also Office of Coal Research, Progress Rept. STD Corp., Aug.-Sept. 1973.

[19]Daily, J.W., "Boundary Layer Phenomena in Combustion Driven MHD Power Generators," Ph.D. Thesis, Dept. of Mech. Eng., Stanford Univ., Stanford, Calif., Dec. 1975.

[20]Brederlow, G., Riedmuller, W. and Salvat, M., "On the Applicability of the Line Reversal Method for Measuring the Electron Temperature in a Weakly Ionized Alkali-Seeded Rare Gas Plasma," Institute für Plasmaphysik, Garching bei München, Germany, Rept. IPP 3/69, Feb. 1968.

[21]Daily, J.W. and Kruger, C.H., "Effect of Cold Boundary Layers on Spectroscopic Temperature Measurements in Combustion Gas Flows," AIAA Paper No. 76-134, Jan. 1976.

[22]McGregor, D.D., "Electron Nonequilibrium in a Supersonic Expansion of Ionized Gas," Institute for Plasma Research, Stanford Univ., Stanford, Calif., Rept. 474, July 1972.

[23]Self, S.A., "Laser Doppler Velocimetry in MHD Boundary Layers," *Proceedings of the 14th Symposium, Engineering Aspects of Magnetohydrodynamics,* April 1974, The University of Space Institute, Tullahoma, Tenn.

[24]Hohnstreiter, G.F., "Spectroscopic Investigation of Electron Temperature Distribution in a Nonequilibrium Partially Ionized Flowing Plasma," Institute for Plasma Research, Stanford Univ., Stanford, Calif., Rept. 212, Dec. 1967.

[25]Gessner, F.B. and Jones, J.B., "On Some Aspects of Fully Developed Turbulent Flow in Rectangular Channels," *Journal of Fluid Mechanics,* Vol. 23, 1965.

[26]Hoagland, L. C., "Fully Developed Turbulent Flow in Straight Rectangular Ducts – Secondary Flow, Its Cause and Effect on the Primary Flow," Dept. of Mechanical Engineering, MIT, Cambridge, Mass., TR-2, Sept. 1960.

[27]Brundrett, E. and Bounes, W.D., "The Production and Diffusion of Vorticity in Duct Flow," *Journal of Fluid Mechanics,* Vol. 19, 1964, pp. 375-394.

[28]Veenhuizen, S.D. and Meroney, R.N., "Secondary Flow in the Entrance Region Boundary Layers of an Expanding Square Duct," ASME Paper No. 72-WA/FE-34, 1972.

[29]Cresi, R.J., Rubin, S.G., Nardo, C.T., and Lin, T.C., "Hypersonic Interaction along a Rectangular Corner," *AIAA Journal,* Vol. 1, Dec. 1969, pp. 2241-2246.

[30]Healzer, J.M., Moffat, R.J. and Kays, W.M., "The Turbulent Boundary Layer on a Rough, Porous Plate: Experimental Heat Transfer with Uniform Blowing," Dept. of Mechanical Engineering, Stanford Univ., Stanford, Calif., Rept. HMT-18, May 1974.

[31]Pimenta, M.M., Moffat, R.J. and Kays, W.M., "The Turbulent Boundary Layer: An Experimental Study of the Transport of Momentum and Heat with the Effect of Roughness," Dept. of Mechanical Engineering, Stanford Univ., Stanford, Calif., Rept. HMT-21, May 1975.

[32]Coney, M.W.E., "Electron-ion Recombination in Seeded Combustion Products," *Journal of Physics, Ser. D: Applied Physics,* Vol. 3, 1970, pp. 1702-1712.